Available online at www.sciencedirect.com
SCIENCE DIRECT®
International Journal of Thermal Sciences 44 (2005) 665–675
International Journal of Thermal Sciences
www.elsevier.com/locate/ijts

Local heat transfer due to several configurations of circular air jets impinging on a flat plate with and without semi-confinement

M. Fenot, J.-J. Vullierme *, E. Dorignac

Laboratoire d'Etudes Thermiques (UMR 6608), 1 Avenue Clement Ader, BP 40109, 86961 Futuroscope Chasseneuil cedex, France

Received 7 July 2004; received in revised form 23 November 2004; accepted 3 December 2004

Available online 3 February 2005

Abstract

A technique based on infrared thermography is used to determine the convective heat transfer on a flat plate on which either a single circular air jet or a row of jets impinged. The flat plate is heated using the thin-foil technique, which enables one to impose different convective heat fluxes. For each flux, a temperature distribution is recorded using a thermographic camera. After that, local heat transfers and local adiabatic temperatures are determined by means of a linear regression method. Parameters that are made to vary include jet injection temperature, the Reynolds number, spacing between adjacent jet, and the distance between the flat plate and jets orifices. In each case, two configurations are investigated: one with and the other without semi-confinement. Results show the independence of heat transfer coefficients and effectiveness from the jet injection temperature within the range studied. The influence of confinement on heat transfer coefficient is weak, but it has a great impact on effectiveness.

Keywords: Impingement; Jets; Thermography; Nusselt number

1. Introduction

Due to its ability to enhance heat transfer, jet impingement is used in a wide range of applications in order to cool, heat or dry surfaces. These applications include glass production, drying of textile and papers, annealing of metals, and cooling of electronic components. Impinging jets are also used in the cooling of particular regions of turbojets such as turbine blades and walls of combustion chambers.

In many of these applications, jet temperature is different from that of the environment in which is issuing. In that case, entrainment of the surrounding fluid into the jet can greatly affect jet temperature and consequently heat transfer from the impingement surface to the jet. Several parameters can affect this entrainment such as the number of jets and the semi-confinement.

Numerous experimental investigations have been performed on flow and heat transfer of jets impinging on flat plate and Jambunathan et al. [1], and Viskanta [2] carried out extensive literature surveys on jet impingement and the influence of different parameters.

But few studies have taken into account the effect of thermal entrainment on heat transfer to impinging jets. Striegl and Diller [3,4] measured heat transfer of up to two slot jets injected into a surrounding fluid whose temperature varied between injection temperature and plate temperature. Other researchers used the adiabatic temperature as a reference to calculate heat transfer coefficients. So, in the case of a single jet, Hollworth and Wilson [5] noticed that for $H/D \geqslant 5$, profiles of dimensionless adiabatic temperature did not depend on Reynolds number and jet-to-plate spacing. With the same apparatus, Hollworth and Gero [6] concluded that if adiabatic temperature is taken as the reference temperature, Nusselt number values are independent from $(T_j - T_\infty)$. Goldstein et al. [7] also used an adimensioned

* Corresponding author. Tel.: (33) 05 49 49 81 33; fax: (33) 05 49 49 81 01.

E-mail addresses: fenot@let.ensma.fr (M. Fenot), jj.vullierme@let.ensma.fr (J.-J. Vullierme).

1290-0729/$ – see front matter
doi:10.1016/j.ijthermalsci.2004.12.002

Nomenclature

D	jet diameter	m
e	impingement plate thickness	m
H	jet exit to impingement plate distance	m
h	heat transfer coefficient on front side	$W{\cdot}m^{-2}{\cdot}K^{-1}$
h_r	heat transfer coefficient on rear side	$W{\cdot}m^{-2}{\cdot}K^{-1}$
Nu	Nusselt number, $= hD/\lambda_{air}$	
P	jet center to center spacing	m
r^2	correlation coefficient of linear regression	
Re	Reynolds number, $= \rho V D/\mu$	
T_{aw}	adiabatic wall temperature	K
T_{inj}	injection wall temperature	K
$T_{w,f}$	front wall temperature	K
$T_{w,r}$	rear wall temperature	K
T_∞	ambient temperature	K
V_{inj}	injection velocity	$m{\cdot}s^{-1}$
X	streamwise coordinate from the center of the jet row	m
Y	spanwise coordinate from the central jet of the row	m
Z	coordinate from the impingement plate	m

Greek symbols

ε_{inj}	injection wall emissivity	
ε_w	impingement wall emissivity	
η	effectiveness, $= (T_{aw} - T_\infty)/(T_j - T_\infty)$	
λ_{air}	air thermal conductivity	$W{\cdot}m^{-1}{\cdot}K^{-1}$
λ_w	wall thermal conductivity	$W{\cdot}m^{-1}{\cdot}K^{-1}$
μ	dynamic viscosity	$Ns{\cdot}m^{-2}$
ρ_{air}	air density	$kg{\cdot}m^{-3}$
σ	Stefan–Boltzmann constant, $= 5.67 \times 10^{-8}$	$W{\cdot}m^{-2}{\cdot}K^{-4}$
$\varphi_{co,f}$	convective heat flux density on the front side	$W{\cdot}m^{-2}$
$\varphi_{co,r}$	convective heat flux density on the rear side	$W{\cdot}m^{-2}$
φ_{elec}	electrical flux density dissipated by Joule effect	$W{\cdot}m^{-2}$
$\varphi_{ra,f}$	radiative heat flux density on the front side	$W{\cdot}m^{-2}$
$\varphi_{ra,r}$	radiative heat flux density on the rear side	$W{\cdot}m^{-2}$

adiabatic temperature: the effectiveness. They showed that it was independent from the Reynolds number and $(T_j - T_\infty)$. Effectiveness decreased with the increasing of jet-to-plate spacing. Baughn et al. [8] used crystal liquid technique and confirmed the results of Goldstein.

Studies concerning a single row of jets are no more numerous than those investigating entrainment effect. Carcasci [9] used a visualisation smoke technique to study the flow of a row of air jets. A series of vortexes and adverse vortexes was observed at the meeting points of the jets. Gardon and Akfirat [10] studied local heat transfer and pressure of a row of slot jets on a flat plate. They pointed out an elevation of heat transfer midway between the jets impingement points. This elevation was visible only for small nozzle-to-plate spacing ($H/D < 6$). For large nozzle-to-plate spacing, loss of the identity of the jets was recorded. Koopman and Sparrow [11] used a naphthalene sublimation technique to measure local Sherwood numbers that can be converted to Nusselt number by employing the heat-mass analogy. Their study involved a row of four jets. Goldstein and Timmers [12] measured heat transfer distribution of a row of three jets on a flat plate using a liquid crystal method. Employing the transient liquid crystal technique, Yan and Saniei [13] investigated heat transfer of a pair of impinging jets and particularly the influence of the jet-to-jet spacing on local heat transfer. In all these studies, jet injection temperature was the same as ambient temperature. The only experimental investigation that dealt with the problem of a row of circular air jets with injection temperature different from the ambient one is that of Goldstein and Seol [14]. Nevertheless, the difference in temperature was weak (less than 20 degrees). Effectiveness was measured by heating the jet flow without heating the plate. The study confirmed that effectiveness is independent from the Reynolds number and $(T_j - T_\infty)$, but dependent on jet-to-plate spacing and of the jet-to-jet distance.

The effect of semi-confinement has been investigated by Obot et al. [19]. They concluded that semi-confinement reduces heat exchanges particularly, with small jet-to-plate spacing. Using Laser Doppler anemometry and liquid crystal, Ashforth-Frost and Jambunathan [20] reported that semi-confinement extends the potential core of a jet and reduces its stagnation point heat transfer.

This study presents an experimental investigation of thermal entrainment with either a single jet or a row of jets. All jets are circular air ones. The jet exit diameter is 10 mm. The range of the different parameters is:

- $H/D = 2; 5;$
- $P/D = 4$ (7 jets); 8 (3 jets);
- $Re = 23\,000;$
- $0 \leqslant X/D \leqslant 7;$
- $20\,^\circ\text{C} \leqslant T_j \leqslant 60\,^\circ\text{C};$
- $20\,^\circ\text{C} \leqslant T_\infty \leqslant 25\,^\circ\text{C}.$

The effect of semi-confinement on impingement heat transfer has also been investigated.

2. Experimental apparatus

The apparatus is shown schematically on Fig. 1. A fan supplies the airflow, which passes through a filtration gear before entering into a heat exchanger. This heat exchanger enables regulation of air temperature from 15 to 70 °C. The flow is then divided between the different jet flows. For each jet, the mass flow rate is measured and controlled by a venturi meters and a valve respectively. Venturi meters and associated pressure converters (JUMO 404304) had been calibrated previously over the mass flow rate used in the experiment.

Fig. 1 also shows the test section. The jet diameter D is 10 mm. The jet injection tubes are 300 mm long. This length is sufficient to obtain a fully developed exit jet flow. The row consists in seven jets. The distance between jets is four times jets' diameter. Four tubes can be blocked to study a row of three jets allowing one to have jet-to-jet spacing distance of eight times the diameter of the jets. In the case of a single jet, only the central jet remains open.

In the semi-confinement configurations, a 300 mm long, 280 mm large and 20 mm thick altuglass plate can be placed at the jet tube exit as shown in Fig. 1. Moreover, two 300 mm long, 20 mm thick lateral plates are positioned perpendicularly to the jets row. Their width depends on distance to plate spacing.

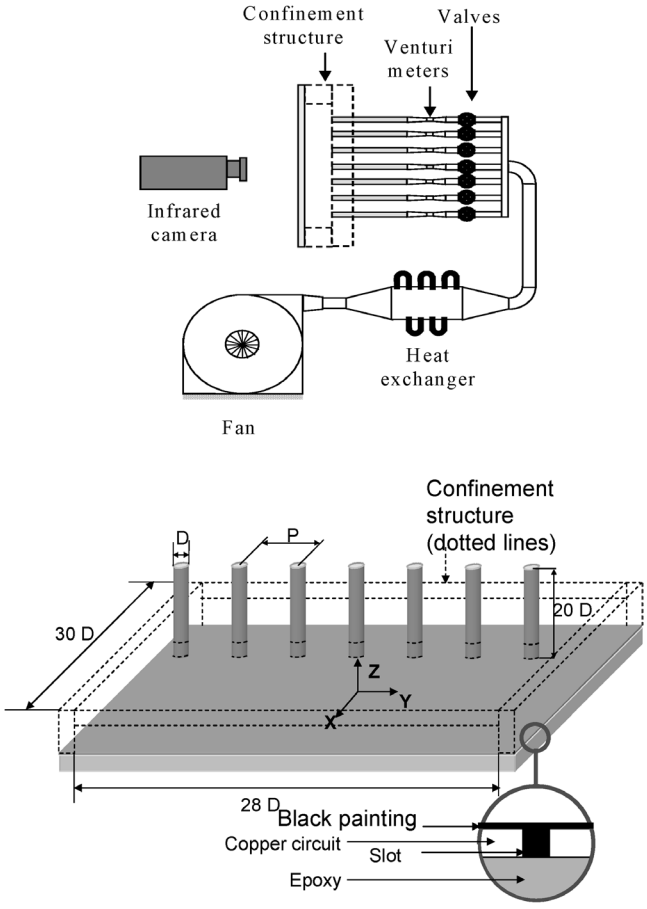

Fig. 1. Experimental apparatus and test section.

Jet temperature is measured at the exit of the tubes using a thermocouple. The temperature scattering between jets is less than 1%. Due to the relatively low jet velocities, Mach number effect is neglected, as shown by Brevet et al. [22].

The impingement plate is rectangular, its spanwise is $30D$ and its streamwise is $28D$. It is made up of epoxy resin whose thickness is 1.6 mm. The plate epoxy thermal conductivity has been measured: $\lambda_w = 0.32\ \mathrm{W{\cdot}m^{-1}{\cdot}K^{-1}} \pm 8 \times 10^{-3}$ with expanded uncertainty for 95% confidence level. A thin foil (17.5 μm thick) of copper covers the epoxy resin on the impingement side. Two electric circuits are engraved in it. They can heat the plate by Joule effect. The width of each circuit varies to provide a non-uniform heat flux density. This way, plate temperature is kept more uniform, reducing heat conduction along the plate. Moreover, the difference in temperatures between plate and jets can be kept as high as possible. This large difference allows one to obtain a flux between jet and plate much greater than other fluxes (radiative ...) and so to achieve higher accuracy in the determination of heat transfer coefficients. Temperature variation resistivity is taken into account in calculus of the heat fluxes. The impingement plate is painted in black (forward and backward) to have high uniform emissivity for precise radiative heat flux calculation and for thermographic measurement. An infrared camera (CEDIP Jade Irfpa) measures the backward temperature of the plate. In this study pertaining to steady state, each thermographic image is the result of the mean of 32 images recorded during 10 s. This mean allows one to remove measurement noise.

3. Procedure

Heat transfer coefficient h and wall adiabatic temperature T_{aw} are measured using infrared thermography coupled with the heated-thin-foil technique. This technique consists in heating electrically the impingement plate using cooper circuits. It enable one to calculate the exact electrical flux density dissipated by Joule effect φ_{elec}. Radiative and convective losses must be taken into account to obtain the convective heat flux density on the front side $\varphi_{co,f}$, which is an exchange between the plate and the jets as presented in Fig. 2:

$$\varphi_{co,f} = \varphi_{elec} - \varphi_{co,r} - \varphi_{rad,f} - \varphi_{rad,r} \tag{1}$$

$$\varphi_{co,r} = h_r(T_{w,r} - T_\infty) \tag{2}$$

$$\varphi_{rad,f} = \sigma\varepsilon_w\left(T_{w,f}^4 - T_\infty^4\right) \tag{3}$$

$$\varphi_{rad,f} = \sigma\left(1/\varepsilon_w + 1/\varepsilon_{inj} - 1\right)^{-1}\left(T_{w,f}^4 - T_{inj}^4\right) \tag{3bis}$$

$$\varphi_{rad,r} = \sigma\varepsilon_w\left(T_{w,r}^4 - T_\infty^4\right) \tag{4}$$

Concerning the convective heat flux density on the rear side $\varphi_{co,r}$, a heat transfer coefficient h_r has been measured

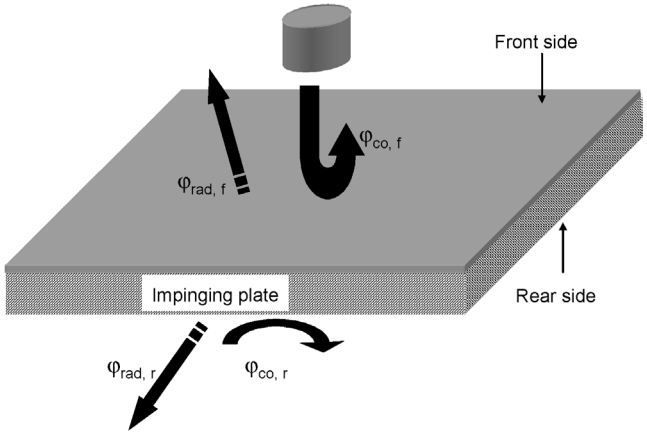

Fig. 2. Heat fluxes.

when all jets are cut off. The dependency of this coefficient has been taken into account. Impingement wall emissivity ε_w and injection wall emissivity ε_{inj} were experimentally calibrated by comparing them with well-known sticky pastille emissivity ($\varepsilon_w = 0.95 \pm 0.02$; $\varepsilon_{inj} = 0.94 \pm 0.02$, both with expanded uncertainty for 95% confidence level). In the configuration without confinement, Eq. (3) is used to calculate front radiative heat flux. When, injection wall is positioned to provide semi-confinement, Eq. (3bis) is used. Radial heat conduction within the impingement wall can be overlooked due to the relatively homogeneous temperature of the plate.

Using adiabatic wall temperature T_{aw} as reference temperature, local heat transfer coefficient on the front side h is defined:

$$h = \varphi_{co,f}/(T_w - T_{aw}) \tag{5}$$

In this case, several studies [7,8,14] have shown that heat transfer coefficient is independent from $(T_j - T_\infty)$. The difficulty when using T_{aw} is to measure it. In many previous studies, the determination of T_{aw} is achieved by measuring the temperature of an isolated plate without heating. And yet, this method is satisfactory only for an injection temperature close to ambient temperature. Otherwise, losses cannot be overlooked and the temperature measured is no longer T_{aw}. Another solution consists in calculating jointly h and T_{aw}. To do so, we can write Eq. (5) as follow:

$$T_w = \varphi_{co,f}/h + T_{aw} \tag{6}$$

And then, for each configuration, four different electrical flux densities are injected. For each electrical flux, cartography of wall temperature T_w is performed using infrared camera. For one point, the couple ($\varphi_{co,f}$, T_w) is to be noted four time. These four couples are placed on a diagram (flux, temperature). Eq. (6) is linear, so performing a linear regression, $1/h$ will be the slope and T_{aw} the y-intercept.

Local heat transfer coefficient h and adiabatic wall temperature T_{aw} are adimensioned as shown in Eqs. (7) and (8).

$$Nu = hD/\lambda_{air} \tag{7}$$

$$\eta = (T_{aw} - T_\infty)/(T_j - T_\infty) \tag{8}$$

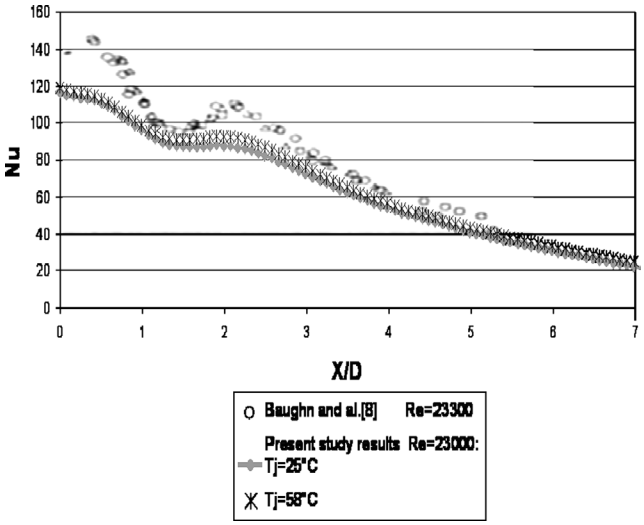

Fig. 3. Nusselt number for 1 jet, $Re = 23\,000$, $H/D = 2$.

Air thermal conductivity λ_{air} is calculated for the adiabatic temperature T_{aw}. In any event, the influence of the temperature chosen to calculate λ_{air} is relatively small [18].

Uncertainties are calculated using a statistical approach [23]. Taking into account errors due to ambient and injection temperature, to electrical, radiative and convective fluxes, and to emissivities, random uncertainty for the Nusselt number values is no higher than 6% and that for effectiveness is no higher than 5%. Overall uncertainty for the Nusselt number values is no higher than 12% and that for effectiveness is no more than 6%. All these uncertainty values have been reported at a 95% confidence level.

4. Results and discussion

The presentation of results will start with those for a single jet, then, results for rows of seven and three jets will be set forth and compared to those for one. Last by, comparison will be made of jets with and without confinement.

4.1. Single jet

Single jet experiments have been conducted for a Reynolds number of 23 000, impingement distances of $H/D = 2$ and 5, and injection temperatures ranging from 22 to 58 °C.

Fig. 3 shows a typical example of local Nusselt numbers. We can see that Nusselt number is independent from $(T_j - T_\infty)$. For $H/D = 2$, we can observe two Nusselt number maxima: one at the stagnation point and the other at approximately $X/D = 2$. For $H/D = 5$, the second maximum is no longer observed. The existence of the second maximum for small jet-to-plate ($H/D < 4$) spacing is generally attributed to the disappearance of secondary vortex structures (Buchlin [21]). These structures most likely break up for greater H/D because of oscillations around the stagnation point increasing with H/D.

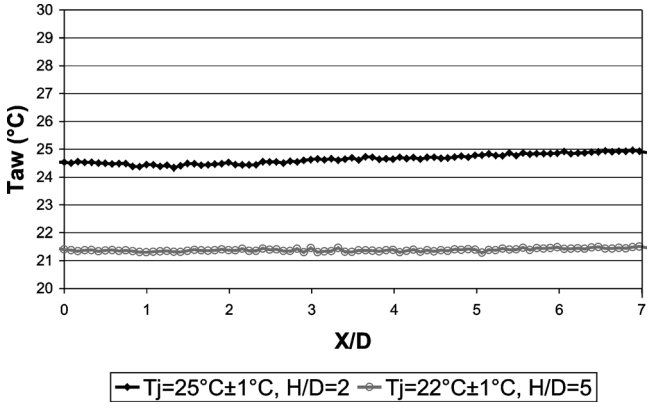

Fig. 4. Taw (°C) for 1 jet, $Re = 23\,000$, $T_\infty = T_j$.

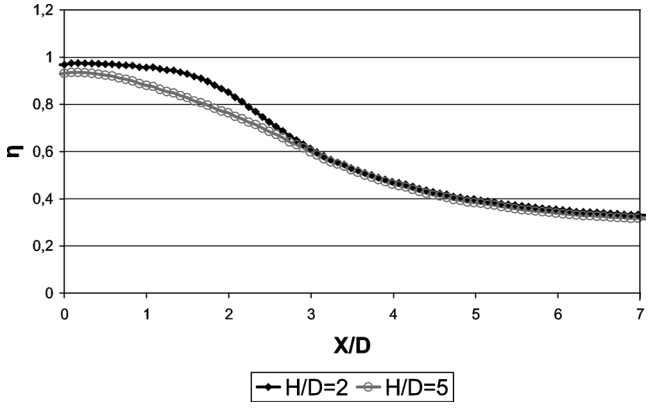

Fig. 5. Effectiveness for 1 jet, $Re = 23\,000$, $T_j = 58\,°C$.

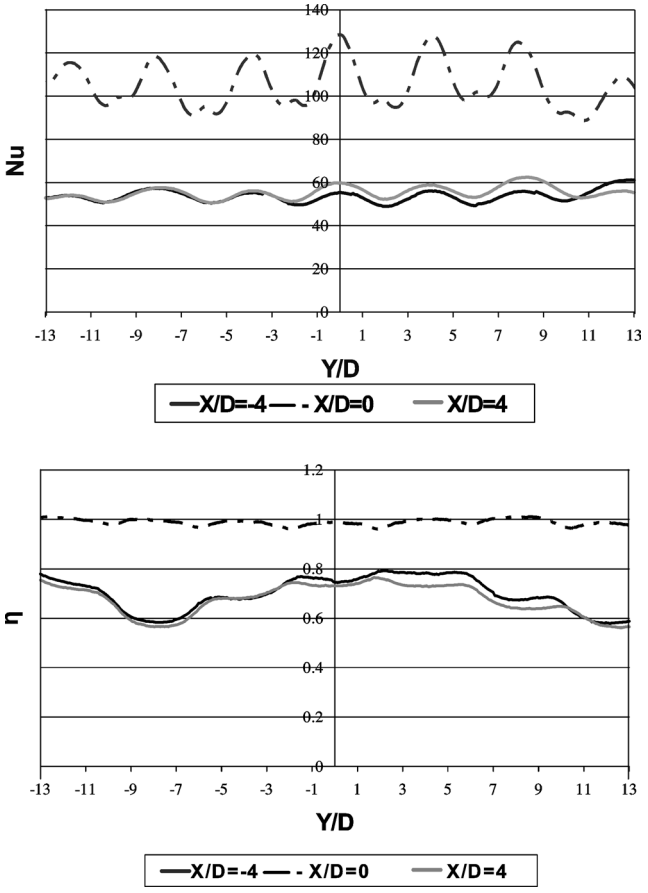

Fig. 6. Symmetry and periodicity of Nusselt number and effectiveness for 7 jets, $Re = 23\,000$, $H/D = 2$, $T_j = 64\,°C$.

These distributions are relatively similar to those observed in other works [8,15]. Comparison with a study by Baughn et al. studies [8] is shown in Fig. 3 for $H/D = 2$. We can notice that local minima and maxima are localized at the same distance from stagnation point. Nusselt number values are slightly different, but, these discrepancies can be explained by the difference of jet pipe diameters (26 mm for Baughn et al. study, and 10 mm for our study), which entails a difference of flow speed. Moreover, the respective experimental techniques are dissimilar. Finally, the Nusselt number value differences are lesser than uncertainties.

In Fig. 4, we can observe local adiabatic temperatures T_{aw} along the test plate for two injection-to-plate distances for an injection temperature T_j equal to ambient temperature T_∞. These temperatures are constant and equal to injection temperature T_j. This result is not surprising, as ambient temperature T_∞ is equal to T_j, the surrounding air entrained by the jet does not modify the temperature of the latter.

Fig. 5 presents the effectiveness η for two hot jets with $T_j \neq T_\infty$. η is slightly lower for $H/D = 5$ than for $H/D = 2$ at stagnation point. In both cases, η is less than 1. In fact, before impingement, the jet melts with surrounding air, and such entrainment decreases its temperature. Jet temperature fall is more important with increasing injection-to-plate distance because the entrainment occurs over a greater length.

For both H/D, η is at a maximum at the stagnation point and then decreases along the plate. In fact, after impingement, the jet continues to drag along ambient air, so effectiveness η continues to decrease with increasing X/D. We can notice that for X/D greater than 3, effectiveness for $H/D = 2$ and for $H/D = 5$ are nearly equal. Before this absciss, the difference in decrease between the two curves could be explained by the existence of large vortexes for small H/D, whereas for greater H/D the flow becomes more chaotic [16].

4.2. Row of jets

A row of seven jets will be studied. In order to confirm the periodicity of the row and the symmetry between the two sides (positive and negative X/D), Fig. 6 shows Nusselt numbers and effectiveness for various X/D. We can see that end effects affect only the two extreme jets and that the symmetry is relatively satisfactory. Therefore, we have only studied the area bounded by $0 \leqslant Y/D \leqslant 2$.

Examples of the cartographies of Nusselt number and effectiveness are displayed in Fig. 7. On the right side of each mapping, we may observe a white disc used as a spatial reference. Iso-values are represented by white lines. We equally note that for large X/D value heat exchange is independent

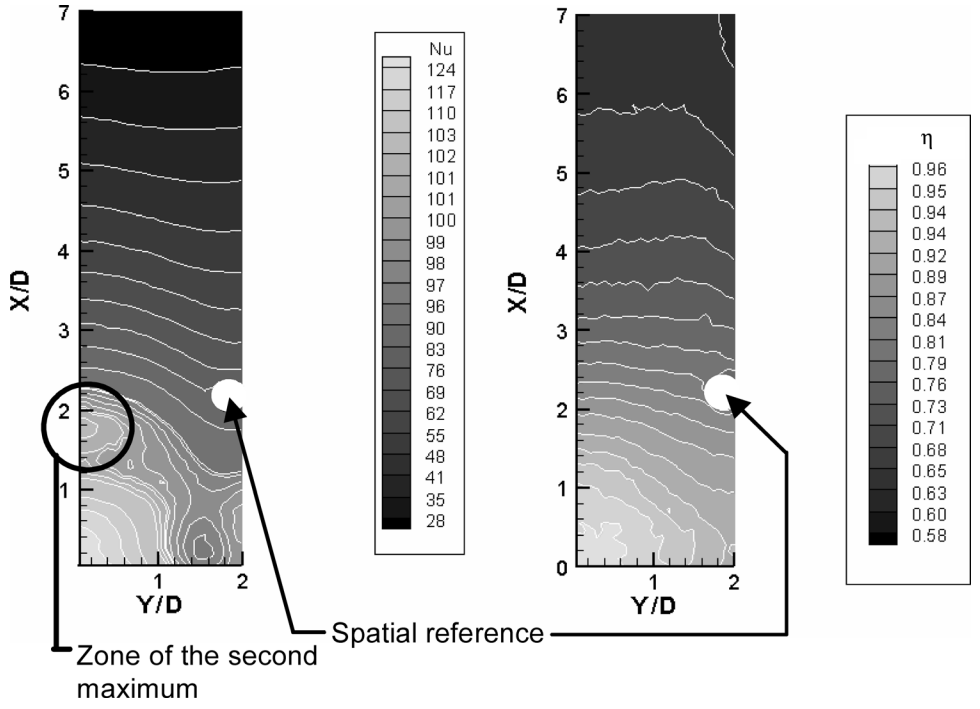

Fig. 7. Local Nusselt number and effectiveness for 7 jets, $Re = 23\,000$, $H/D = 2$, $T_j = 64\,^{\circ}\mathrm{C}$.

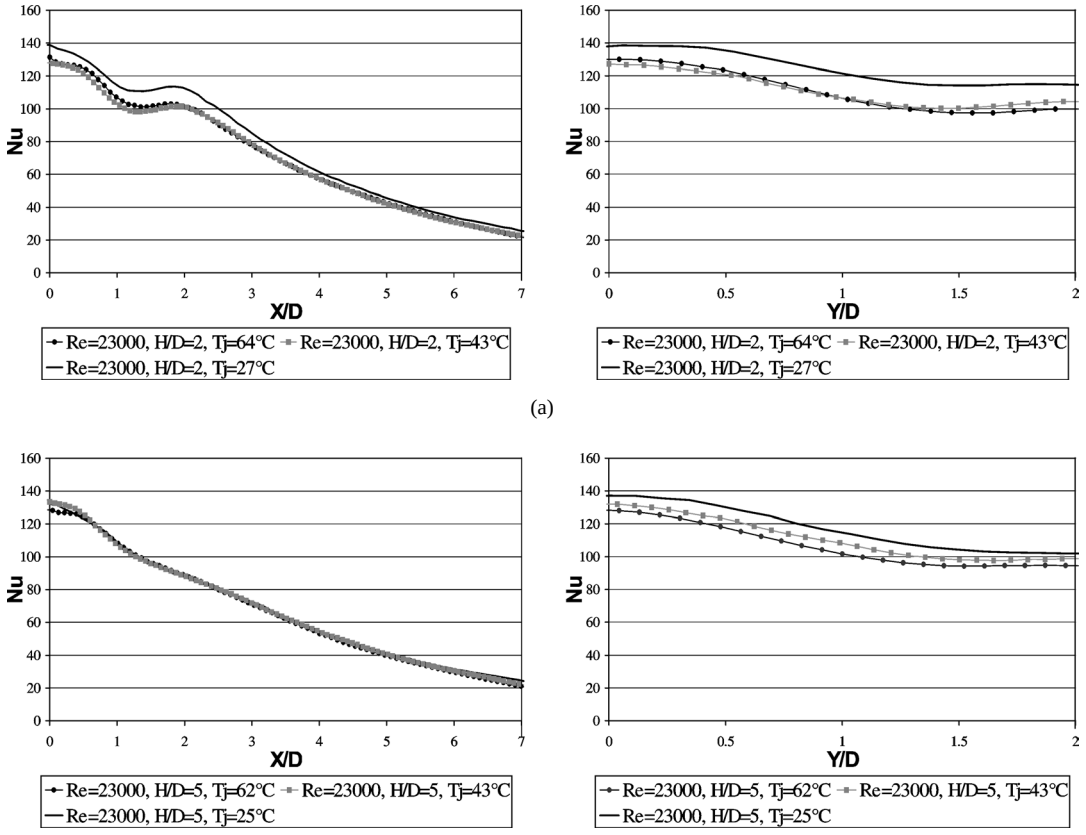

Fig. 8. Local Nusselt numbers for 7 jets along streamwise and spanwise for $Re = 23\,000$ and: (a) $H/D = 2$; (b) $H/D = 5$.

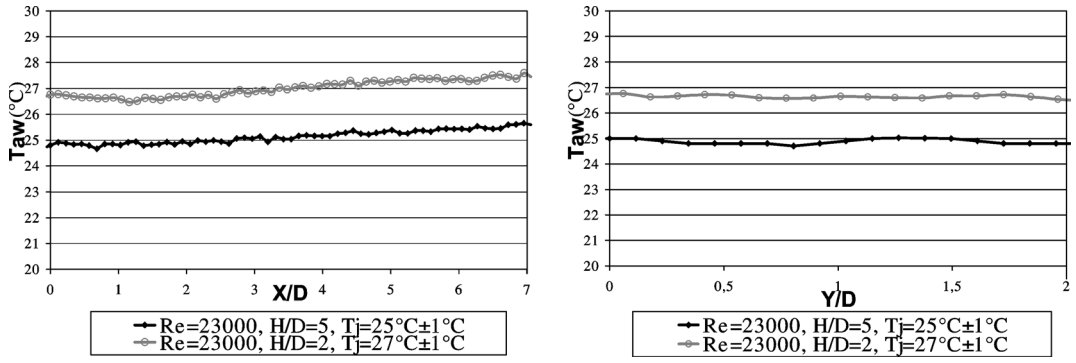

Fig. 9. Taw (°C) for 7 jets, $Re = 23\,000$, $T_j = T_\infty$.

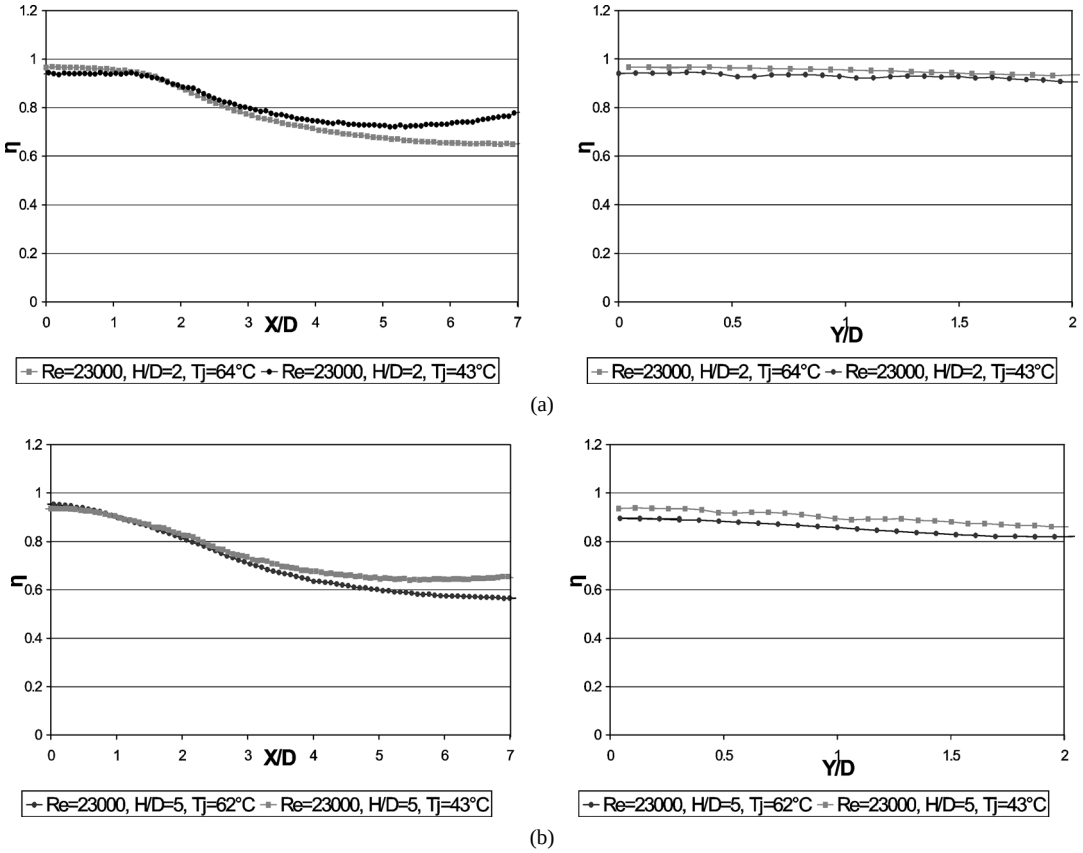

Fig. 10. Effectiveness for 7 jets along streamwise and spanwise for $Re = 23\,000$ and: (a) $H/D = 2$; (b) $H/D = 5$.

of Y/D. Jet flows are no longer distinct from one to another, there is only a unique wall jet flow.

Fig. 8 presents local Nusselt numbers, for various configurations, along the spanwise and streamwise axes. As in one-jet experiments, values of local Nusselt number for a row of 7 jets appear to be independent from $(T_j - T_\infty)$ (the differences between configurations of various injection temperatures are lower than uncertainty). For both injection-to-plate distances, a maximum is visible at the stagnation point. For $H/D = 2$, as with a single jet, a second maximum is visible for $X/D = 2$. But, unlike a single in which maximum is visible all around the impinging point, for a row it can only be noticed around the X axis for $Y/D < 0.6$ as shown in Fig. 7. If this second maximum is due to disappearance of secondary vortexes, then interaction between contiguous jets may be preventing these vortexes from appearing and so the maximum no longer exists in region where interactions are strong, $(Y/D > 0.6)$. The maximum amount of heat exchange midway between the jets observed by many authors [10–12] is far from obvious. A small increase in local Nusselt number value is perceptible only for $H/D = 2$. The maximum is generally attributed to the fountain effect; it is more prominent for small injection-to-plate spacing and jet-to-jet spacing. Perhaps, current Reynolds number is too small and impingement distance too high to produce more than a very small increase of heat exchange. For high

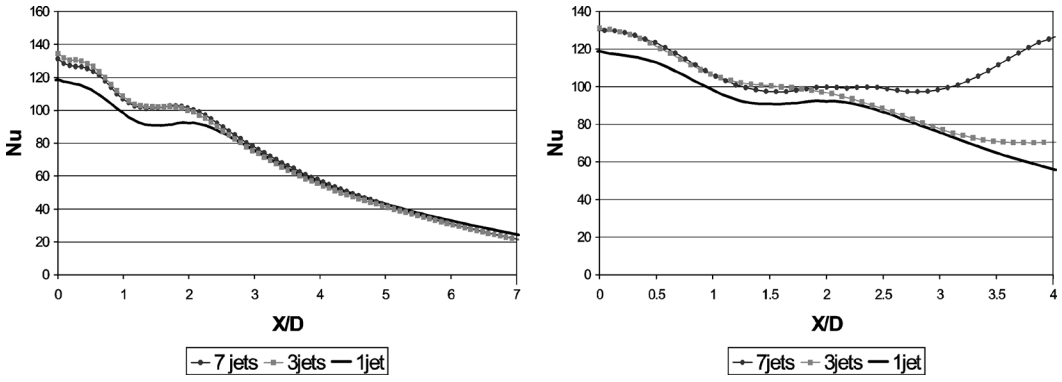

(a)

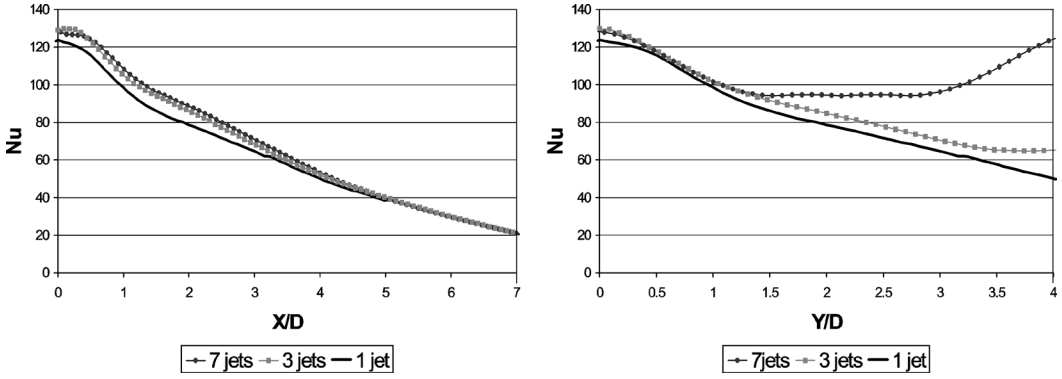

(b)

Fig. 11. Local Nusselt number comparison of 1, 3, 7 jets for $Re = 23\,000$, $T_j \approx 60\,^{\circ}\mathrm{C}$ and: (a) $H/D = 2$; (b) $H/D = 5$.

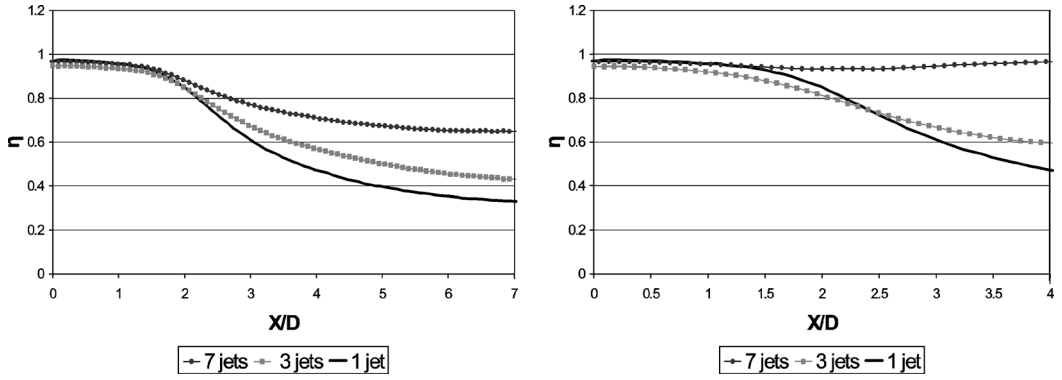

(a)

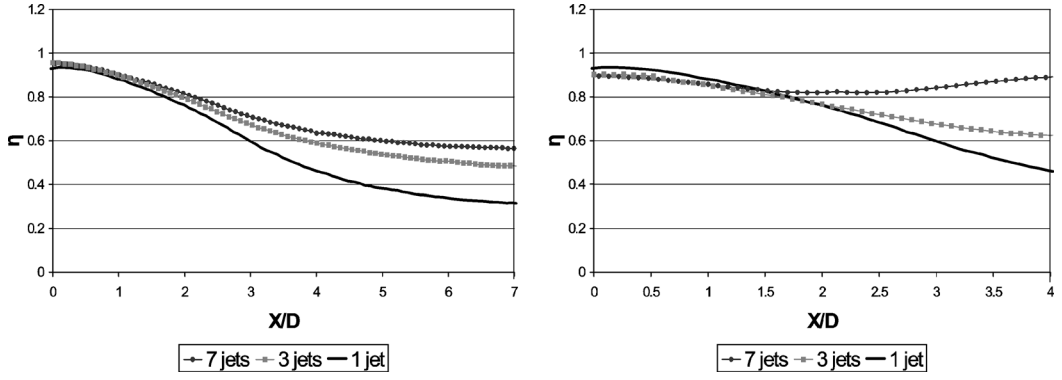

(b)

Fig. 12. Effectiveness comparison of 1, 3, 7 jets for $Re = 23\,000$, $T_j \approx 60\,^{\circ}\mathrm{C}$ and: (a) $H/D = 2$; (b) $H/D = 5$.

streamwise spacing ($X/D > 5$ or 6) jets are no longer differentiated and become a two-dimensional wall flow. For a given distance to stagnation point, local Nusselt number value is higher for low X/D (highest Nusselt number is for $X/D = 0$). In fact, interaction between jets seems to reduce velocity field and heat exchanges as well.

As expected, when injection temperature T_j is equal to ambient temperature T_∞, T_{aw} remains constant and equal to T_j (Fig. 9). Concerning configurations with T_j different from T_∞, variations of effectiveness along streamwise and spanwise are displayed in Fig. 10. Effectiveness seems independent from $(T_j - T_\infty)$. For both impingement distances, η decreases with increasing X/D, probably for the same reasons as for a single jet. On the other hand, η is practically independent from Y/D, indeed effectiveness decrease is lower than 0.07 for $H/D = 5$ and to 0.04 for $H/D = 2$. A possible explanation is that interaction between adjacent jets breaks the jet vortexes that enhance melting of a jet and the surrounding air.

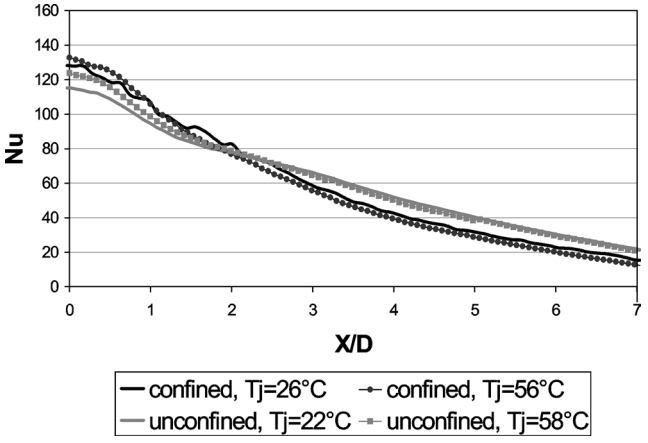

Fig. 13. Local Nusselt numbers comparison of 1 jet for $Re = 23\,000$, $H/D = 5$.

4.3. Comparison between single jet and rows of 3 and 7 jets

To study the influence of the jet-to-jet spacing P/D, it is possible to cut off air feed from four jets. In that case, there remain three jets and consequently $P/D = 8$, whereas $P/D = 4$ for 7 jets. Fig. 11 shows local Nusselt number for 1, 3 and 7 jets. Along the X-axis, variations of Nusselt number for three and for seven jets are nearly the same. The Nusselt number distribution for 1 jet is slightly different but this difference is lower than measure uncertainty. In fact, it seems that for $X/D = 0$ influence of adjacent jets is negligible whichever jet-to-plate placing is used. Along the Y-axis, distributions of local Nusselt number are identical for one, three and seven jets up until $Y/D = 2$, then, the seven jets distribution diverges from the other. For $Y/D > 3$, the three jets distribution becomes constant due to interaction with the

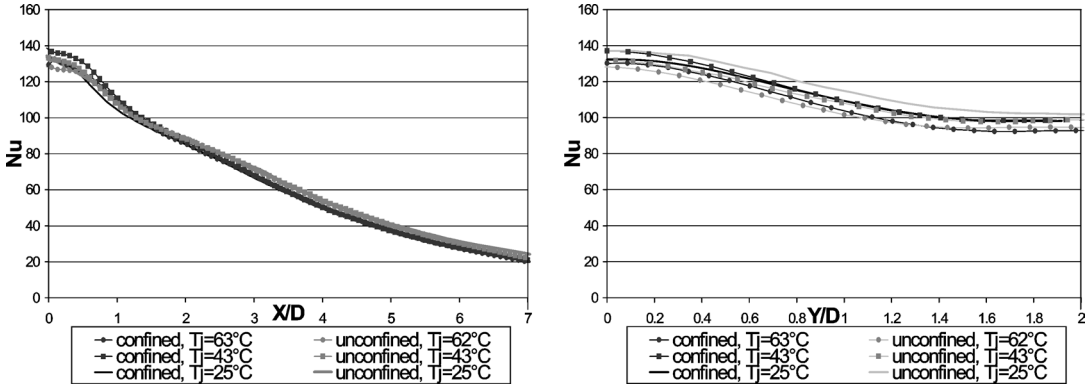

Fig. 14. Local Nusselt numbers comparison of 7 jets for $Re = 23\,000$, $H/D = 5$.

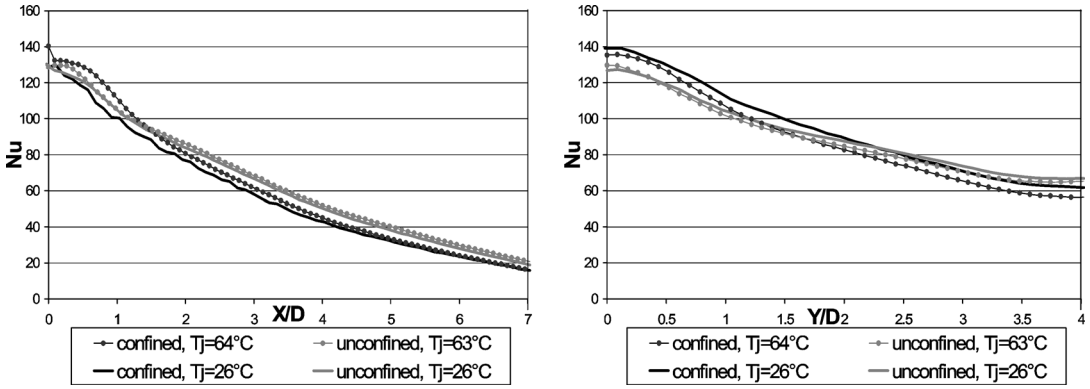

Fig. 15. Local Nusselt number comparison of 3 jets for $Re = 23\,000$, $H/D = 5$.

adjacent jet, whereas one jet distribution continues to decrease. So, the influence of adjacent jets seems to be limited away from the region of jets encounter, around $Y/D = 2$. Considering these results with regard to optimization, we may conclude that the multiplication of jets increases the heat transfers slightly but enlarge the mass flow rate greatly. As recorded by Brevet et al. [17], the ratio between average Nusselt number and mass flow rate seems to grow with increasing distance between jets.

At the stagnation point, effectiveness has the same value for whichever number of jets (Fig. 12). Along the X-axis, effectiveness decrease is greater for one jet, then for three and finally for seven. Along the spanwise, effectiveness decreases for 3 jets, whereas it is constant for seven jets. So it seems that more surrounding air is mixed with jet flow for one jet than for 3 jets, and for 3 jets than for 7 jets.

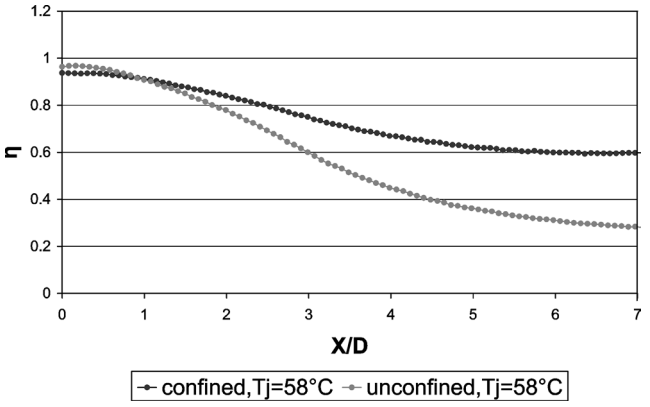

Fig. 16. Effectiveness comparison of 1 jet for $Re = 23\,000$, $H/D = 5$.

4.4. Comparison between confined and unconfined configurations

Figs. 13–18 display comparison between confined and unconfined configurations for $H/D = 5$. Results for $H/D = 2$ are not presented but are similar to those for $H/D = 5$. As regards Nusselt number, differences between confined and unconfined arrangement are rather small. At stagnation point, we can observe that heat transfer is greater for confined cases. But with increasing distance from stagnation point along X axis as along Y axis, Nusselt number distribution becomes higher for unconfined configuration. This is particularly patent for one jet and can be noticed for 3 and 7 jets as well.

The confinement influence on effectiveness is much stronger. In the case of one jet, the decrease of effectiveness distribution with increasing distance from stagnation point is much more pronounced for unconfined than for confined arrangement than. When the jet flow is cooled by dragging ambient air, it heats the latter. And, we can suppose that in confined configuration, surrounding air is trapped between

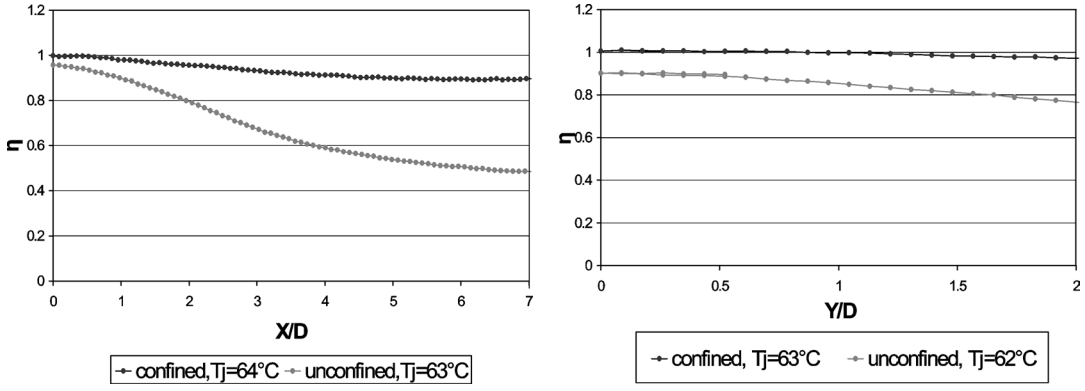

Fig. 17. Effectiveness comparison of 7 jets for $Re = 23\,000$, $H/D = 5$.

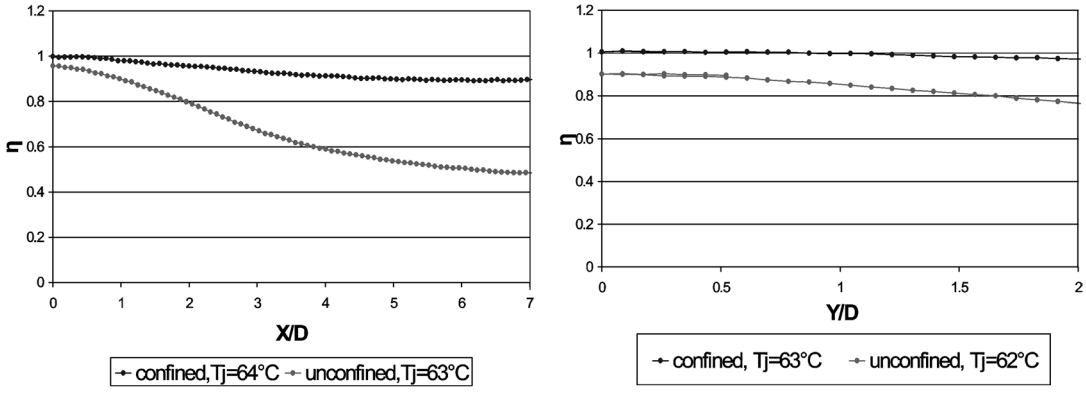

Fig. 18. Effectiveness comparison of 3 jets for $Re = 23\,000$, $H/D = 5$.

injection and impact plate. So, the surrounding air temperature rises and jet flow temperature is not as cooled as in the case of unconfined configuration.

For a row of jets with 3 or 7 of them either, effectiveness is almost constant as in the case when jet temperature is equal to surrounding air temperature. In fact, as in the one jet case, ambient air is heated by jet flow. But due to the fountain effect resulting from the interaction of adjacent jets, the phenomenon is more pronounced and ambient air temperature become equal to jets injection temperature.

5. Conclusion

By injecting four different flux densities and by performing a cartography of the impinging plate for each flux density, it is possible to determine both local heat transfer coefficients (and then local Nusselt number) and the local adiabatic temperature that is the reference temperature used.

First of all, a single jet was studied to validate our experimental method. Local Nusselt number values were compared with those of other studies and have proved to be similar. Local Nusselt number and effectiveness were also shown to be independent from $(T_j - T_\infty)$.

Then a row of jets was studied. Whichever jet-to-jet distance is studied, local Nusselt number distributions are approximately identical to those of a single jet. In fact, the neighbouring jets influence over Nusselt number values is limited to a region situated midway between jets ($Y \approx P/2$). On the other hand, effectiveness distribution greatly depends on the jet-to-jet distance: its decrease is more pronounced for small jet-to-jet spacing P/D.

Finally, a comparison between confined and unconfined configurations was performed with for 1, 3 and 7 jets. In all cases, Nusselt number cartographies remain approximately about the same with or without confinement. However, effectiveness variations are clearly different for configurations with as opposed to without confinement. Effectiveness decreases more rapidly for the configuration without confinement.

Acknowledgements

This study has been carried out as part of the ARCAE research programme financed by DGA, ONERA, SNECMA moteurs and TURBOMECA. Their support is acknowledged gratefully.

References

[1] K. Jambunathan, E. Lai, M.A. Moss, B.L. Button, A review of heat transfer data for single circular impingement, Internat. J. Heat Fluid Flow 13 (2) (1992) 106–115.

[2] R. Viskanta, Heat transfer to impinging isothermal gas and flame jets, Experimental Thermal Fluid Sci. 6 (1993) 111–134.

[3] S.A. Striegl, T.E. Diller, The effect of entrainment temperature on jet impingement heat transfer, J. Heat Transfer 106 (1984) 27–33.

[4] S.A. Striegl, T.E. Diller, An analysis of the effect of entrainment temperature on jet impingement heat transfer, J. Heat Transfer 106 (1984) 804–810.

[5] B.R. Hollworth, S.I. Wilson, Entrainment effects on impingement heat transfer: Part I: Measurements of heated jet velocity and recovery temperatures on target surface, Heat Transfer 106 (1984) 797–803.

[6] B.R. Hollworth, L.R. Gero, Entrainment effects on impingement heat transfer: Part II: Local heat transfer measurements, Trans. ASME 107 (1985) 910–915.

[7] R.J. Goldstein, K.A. Sobolik, W.S. Seol, Effect of entrainment on the heat transfer to a heated circular air jet impinging on a flat surface, Trans. ASME 112 (1999) 608–611.

[8] J.W. Baughn, A.E. Hechanova, X. Yan, An experimental study of entrainment effects on the heat transfer from a flat surface to a heated circular impinging jet, J. Heat Transfer 113 (1991) 1023–1025.

[9] C. Carcasci, An experimental investigation on air impinging jets using visualisation methods, Internat. J. Thermal Sci. 38 (1999) 808–818.

[10] R. Gardon, J.C. Akfirat, Heat transfer characteristics of impinging two-dimensional air jets, J. Heat Transfer 88 (1966) 101–108.

[11] R.N. Koopman, E.M. Sparrow, Local and average transfer coefficients due to an impinging row of jets, Internat. J. Heat Mass Transfer 19 (1976) 673–683.

[12] R.J. Goldstein, J.F. Timmers, Visualisation of heat transfer from arrays of impinging jets, Internat. J. Heat Mass Transfer 25 (12) (1982) 1857–1868.

[13] X. Yan, N. Saniei, Measurments of local heat transfer coefficients from a flat plate to a pair of circular air impinging jets, J. Experimental Heat Transfer 9 (1) (1996) 29–47.

[14] R.J. Goldstein, W.S. Seol, Heat transfer to a row of impinging circular air jets including the effect of entrainment, Internat. J. Heat Mass Transfer 34 (8) (1991) 2133–2147.

[15] J.W. Baughn, S. Shimizu, Heat transfer measurements from a surface with uniform heat flux and an impinging jet, Trans. ASME 111 (1989) 1096–1098.

[16] C.O. Popiel, O. Trass, Visualisation of a free and impinging round jet, Experimental Thermal Fluid Sci. 4 (1991) 253–263.

[17] P. Brevet, C. Dejeu, E. Dorignac, M. Jolly, J.J. Vullierme, Heat transfer to a row of impinging jets in consideration of optimisation, Internat. J. Heat Mass Transfer 45 (2002) 4190–4200.

[18] P. Brevet, Etude expérimentale et numérique des transferts thermiques par impact de jet, application aux moteurs aéronautiques, Thesis, University of Poitiers, France, 2001.

[19] N.T. Obot, W.J.M. Douglas, A.S. Mujumdar, Effect of semi-confinement on impingement heat transfer, in: 7th Int. Heat Transfer Conf., Munich, 1982, pp. 395–400.

[20] S. Ashforth-Frost, K. Jambunathan, Effect of nozzle geometry and semi-confinement on the potential core of a turbulent axisymetric jet, in: 10th Int. Heat Transfer Conf., Brighton, 1994.

[21] J.M. Buchlin, Convective heat transfer in impinging gas jet systems, in: Aero-Thermal Performance of Internal Cooling Systems in Turbomachines, in: VKI for Fluids Dynamics Lecture, Series 2000-03, 2000.

[22] P. Brevet, E. Dorignac, J.J. Vullierme, Mach number effect on jet impingement heat transfer, in: Heat Transfer in Gas Turbine Systems, in: Ann. of New York Acad. Sci., vol. 934, New York Academy of Sciences, New York, 2000, pp. 409–416.

[23] Estimation des incertitudes de mesure, Laboratoire National d'Essais, Bureau Qualité-Statistiques, 1997.